Electronic Supplementary Material (ESI) for Nanoscale.

Supplementary Information: Optical cooling of lead halide perovskite nanoparticles enhanced by Mie resonances

Pavel A. Tonkaev, George P. Zograf, and Sergey V. Makarov*

Faculty of Physics and Engineering, ITMO University, St. Petersburg, 197101, Russia

E-mail: s.makarov@metalab.ifmo.ru

Contents

I. Modeled and experimental dielectric permittivity

II. Absorption cross-section calculation

III. Purcell factor calculation

IV. Purcell factor for NP in glass

V. NP Temperature Calculation

VI. Carrier generation inside the NP

VII. Surface recombination in perovskite

VIII. Numerical modelling description

IX. GaAs Purcell factor, absorption cross-section and optical heating calculations

X. Numerical modeling for film

I. Modeled and experimental dielectric permittivity

The considered permittivity for this work was derived according to the Eq. 7 of the manuscript. Only excitonic contribution was taken into account in imaginary part, which, we believe, is reasonable in the near-IR region (red-shifted from the λ_{PL}). Comparison of experimental[S1] and derived permittivities is presented in the Fig. S1. Parameters for the Eq. 7 have been determined via fitting of the experimental excitonic absorption without the contribution of the interband and free-carriers absorption with the one obtained from the calculation.

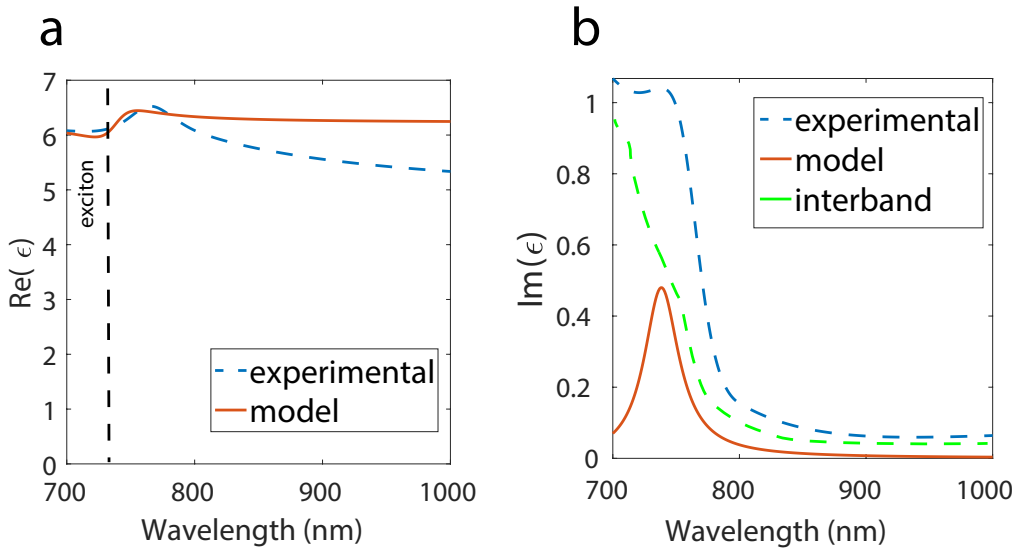

Figure S1: **$MAPbI_3$ permittivity.** Modeled and experimental permittivity for $MAPbI_3$: real (a) and imaginary (b) parts.

We believe, that the losses possessed by the $MAPbI_3$ perovskite films are slightly over-valued. This can be explained by the height inhomogeneity of the films prepared chemically. Indeed, the alteration of the height can be of the order of 20nm[S2], thus causing parasitic Rayleigh scattering from the surface which contributes to the total 'absorption'.

II. Absorption cross-section calculation

Absorption cross-section σ_{abs}) of spherical NPs was calculated using Mie-theory[S3,S4]. σ_{abs} is linked with extinction and scattering cross-sections $\sigma_{abs} = \sigma_{ext} - \sigma_{sca}$, where σ_{ext} and σ_{sca} are following:

$$\sigma_{sca} = \frac{W_{sca}}{I} = \frac{2\pi}{k^2}\sum_{n=1}^{\infty}(2n+1)(|a_n|^2 + |b_n|^2), \tag{S1}$$

$$\sigma_{ext} = \frac{W_{ext}}{I} = \frac{2\pi}{k^2}\sum_{n=1}^{\infty}(2n+1)Re(a_n + b_n), \tag{S2}$$

where W_{sca}, W_{ext} are the scattered and extinct energies by the nanosphere, respectively, $k = 2\pi\sqrt{\epsilon}/\lambda$, ϵ is the dielectric permittivity, I is the incident intensity, a_n and b_n are the scattering Mie-coefficients that describe interaction of the NP with a plane wave. The coefficients for the case of equally non-magnetic surrounding media and NP can be derived from the following expressions:

$$a_n = \frac{m\psi_n(mx)\psi_n'(x) - \psi_n(x)\psi_n'(mx)}{m\psi_n(mx)\xi_n'(x) - \xi_n(x)\psi_n'(mx)}, \tag{S3}$$

$$b_n = \frac{\psi_n(mx)\psi_n'(x) - m\psi_n(x)\psi_n'(mx)}{\psi_n(mx)\xi_n'(x) - m\xi_n(x)\psi_n'(mx)}, \tag{S4}$$

where $x = \frac{kD}{2}$, D is the NP diameter, m is the relative refractive index of the sphere and the Riccati-Bessel functions : $\psi_n(\rho) = \rho j_n(\rho)$, $\xi_n(\rho) = \rho h_n^{(1)}(\rho)$, where j_n and $h_n^{(1)}$ are spherical Bessel and Hankel functions, respectively.

III. Purcell factor calculation

Calculation of the emission rate of a dipole source placed inside a homogeneous dielectric sphere is based on the the method described by Chew *et al.*[S5] In order to estimate the emission rate, we employ following expressions for radial oscillation:

$$R^{\perp}/R_0^{\perp} = \frac{3}{2}\frac{\epsilon_1 n_1}{\rho_1^2}\left(\frac{\epsilon_2}{\mu_2}\right)^{1/2}\sum_{n=1}^{\infty}\frac{n(n+1)(2n+1)j_n^2(y_1)}{y_1^2|D_n|^2}, \tag{S5}$$

and for tangential oscillations:

$$R^{\parallel}/R_0^{\parallel} = \frac{3}{4}\frac{\epsilon_1 n_1}{\rho_1^2}\left(\frac{\epsilon_2}{\mu_2}\right)^{1/2}\sum_{n=1}^{\infty}(2n+1)\left(|\frac{(y_1 j_n(y_1))'}{y_1 D_n}|^2 + \frac{\mu_1\mu_2 j_n^2(y_1)}{\epsilon_1\epsilon_2|D_n'|^2}\right), \tag{S6}$$

where $n_1 = \sqrt{\mu_1\epsilon_1}, y_1 = k_1 r', \rho_{1,2} = \frac{k_{1,2}D}{2}$,

$D_n = \epsilon_1 j_n(\rho_1)(\rho_2 h_n^{(1)}(\rho_2))' - \epsilon_2 h_n^{(1)}(\rho_2)(\rho_1 j_n(\rho_1))'$,

$D_n' = \mu_1 j_n(\rho_1)(\rho_2 h_n^{(1)}(\rho_2))' - \mu_2 h_n^{(1)}(\rho_2)(\rho_1 j_n(\rho_1))'$,

r' - radial position of a dipole source inside the dielectric sphere.

The functions j_n and $h_n^{(1)}$ are spherical Bessel and Hankel functions of the first kind.

For uniform distribution of excited atoms density the average emission rates are evaluated as following:

$$\langle R^{\perp}/R_0^{\perp}\rangle = 2H\sum_{n=1}^{\infty}\frac{n(n+1)L_n}{|D_n|^2}, \tag{S7}$$

$$\langle R^{\parallel}/R_0^{\parallel}\rangle = H\sum_{n=1}^{\infty}\frac{M_n}{|D_n|^2} + \frac{K_n G(2n+1)}{|D_n'|^2}, \tag{S8}$$

where $H = (9\epsilon_1/4\rho_1^5)(\mu_1\epsilon_1\epsilon_2/\mu_2)^{1/2}$,

$G = \mu_1\mu_2/\epsilon_1\epsilon_2$,

$K_n = \int_0^{\rho_1}\rho^2 j_n^2(\rho)d\rho = \rho_1^3/2(j_n^2(\rho_1) - j_{n+1}(\rho_1)j_{n-1}(\rho_1))$,

$L_n = (2n+1)\int_0^{\rho_1} j_n^2(\rho)d\rho$,

$M_n = (2n+1)\int_0^{\rho_1}((\rho j_n(\rho))')^2 d\rho$.

The total emission rate can be found in the form:

$$\langle R/R_0\rangle = \langle 2R^{\parallel}/R_0^{\parallel} + R^{\perp}/R_0^{\perp}\rangle/3 = 2H\sum_{n=1}^{\infty}\left(\frac{J_n(2n+1)}{|D_n|^2} + \frac{GK_n(2n+1)}{|D_n'|^2}\right), \tag{S9}$$

where $J_n = K_{n-1} - n\rho_1 j_n^2(\rho_1)$.

IV. Purcell factor for NP in glass

Purcell factor calculation results for nanosphere in homogeneous air media according to Eq. S9 are presented in the main text. For NP in homogeneous glassy environment (n=1.45), lowers optical contrast takes place between the nanosphere material ($MAPbI_3$ in our case) and the surrounding media. Thereby, resonances in the emission spectrum undergo slight shift with decreasing of the Q-factor. Comparison of emission rate in air (red dashed curve) and glass (blue solid curve) is shown in Fig S2. For MO-mode the peak is shifted by 15 nm in NPs diameter and equals to 2.17.

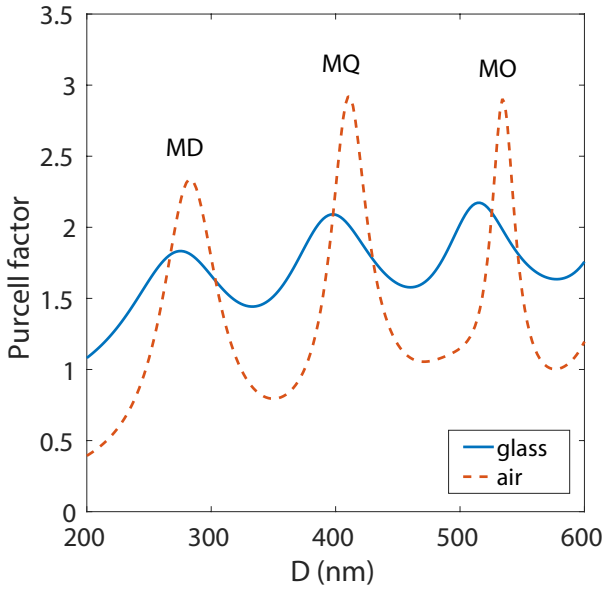

Figure S2: **Pircell factor.** Calculated Purcell factor for NP in glass (blue solid curve) and air (red dashed curve) homogeneous media for 770 nm wavelength.

Since the real experiment is usually carried out with the NP placed on, for instance, a glass substrate, one should take this into account while performing numerical modelling of the experiment. However, in this case the real value of the emission rate lies somewhere in between of 2.89 and 2.17 for MO mode at 770 nm wavelength. Spectral position and the magnitude of the absorption does not undergo significant change while changing the surrounding homogeneous air media to glass substrate[S6,S7].

V. NP Temperature Calculation

Since the laser regime has been selected as a CW for the optical cooling, we consider a steady-state thermal diffusion equation for the temperature distribution $T(\mathbf{r})$:

$$\nabla(\kappa\nabla T) = -q(r) \tag{S10}$$

where κ is the thermal conductivity and $q(r)$ is power the density.

Let's assume that the thermal conductivity κ is homogeneous for the nanosphere and the surrounding space, thus the distribution of the power inside the NP is homogeneous and can be set as a constant $q(r) = q$. Temperature distributions inside (T_1) and outside (T_2) the NP are following:

$$\frac{1}{r^2}\frac{\partial}{\partial r}r^2\frac{\partial T_1}{\partial r} = -\frac{q}{\kappa_1} \quad \text{inside} \quad \text{NP}, \tag{S11}$$

$$\frac{1}{r^2}\frac{\partial}{\partial r}r^2\frac{\partial T_2}{\partial r} = 0 \quad \text{outside} \quad \text{NP}, \tag{S12}$$

where κ_1 is thermal conductivity of the NP.

After some straightforward calculations we derive :

$$T_1 = -\frac{qr^2}{6\kappa_1} - \frac{C_1}{r} + C_1' \quad \text{inside} \quad \text{NP}, \tag{S13}$$

$$T_2 = -\frac{C_2}{r} + C_2' \quad \text{outside} \quad \text{NP}. \tag{S14}$$

We employ boundary conditions for a perfect thermal contact between the the NP and surrounding medium:

$$T_1|_{r=R} = T_2|_{r=R}, \tag{S15}$$

$$-\kappa_1 \frac{\partial T_1}{\partial r}|_{r=R} = -\kappa_2 \frac{\partial T_2}{\partial r}|_{r=R}, \tag{S16}$$

where κ_2 is thermal conductivity of surrounding medium, R is NP radius.

And some physical limitations corresponding to non-infinite solution at the NPs center and constant temperature infinitely distanced from the source:

$$T_2|_{r\to\infty} \to T_0 \Rightarrow C_2' = T_0, \tag{S17}$$

$$T_1|_{r=0} < \infty \Rightarrow C_1 = 0. \tag{S18}$$

The solution of the equation S11 with these boundary conditions gives an expression for the temperature inside the NP with diamater D:

$$T_1 = \frac{P}{4\pi\kappa_1 D}\left(1 - \frac{d^2}{D^2}\right) + \frac{P}{2\pi\kappa_2 D} + T_0, \tag{S19}$$

where $P = \pi D^3 q/6$ is the total absorbed or radiated power, and T_0 is the temperature of the surrounding medium. As the thermal conductivity of NP is much larger than that of surrounding medium (κ_2), i.e. $\kappa_1 \gg \kappa_2$, the temperature inside the NP is homogeneous, which simplifies the expression for the temperature increase inside the NP:

$$\Delta T_{NP} = T_1 - T_0 = \frac{P}{2\pi\kappa_2 D}. \tag{S20}$$

Total power is determined by the difference of absorbed power P_{abs} and radiated power P_{lum}:

$$P = P_{abs} - P_{lum}. \tag{S21}$$

The power absorbed by the NP can be calculated via its absorption cross-section C_{abs} and incident light intensity I:

$$P = C_{abs} I. \tag{S22}$$

The radiated power can be determined by cooling efficiency from equation 11:

$$P_{lum} = (1 + \eta_c) P_{abs} \tag{S23}$$

.

Considering all the above, the temperature change of the NP is following:

$$\Delta T = -\eta_c \frac{I \sigma_{abs}}{2\pi \kappa_2 D}. \tag{S24}$$

VI. Carrier generation inside the NP

Light-induced carrier density for 530 nm $MAPbI_3$ nanosphere under 980 nm wavelength laser illumination of different intensities is shown in Fig. S3a. The results depict the solution of Eq.10 from the main text. The highest optical cooling is observed at carrier density $N = 3\ 10^{18}\ cm^{-3}$. For higher carrier densities Auger recombination starts to dominate and cooling efficiency decreases.

According Eq.9 and Eq.11 from main text external quantum efficiency is determined as:

$$\eta = \frac{BF_pN^2}{AN + BF_pN^2 + CN^3}, \tag{S25}$$

where A is monomolecular recombination coefficient, B is bimolecular recombination coefficient and C is trimolecular recombination coefficient. Calculated photoluminescence quantum efficiency for pump with 980 nm wavelength is presented in Fig. S3b. Blue curve is calculated internal quantum efficiency ($F_p = 1$) and red curve is external quantum efficiency for 530 nm $MAPbI_3$ NP taking into account Purcell factor.

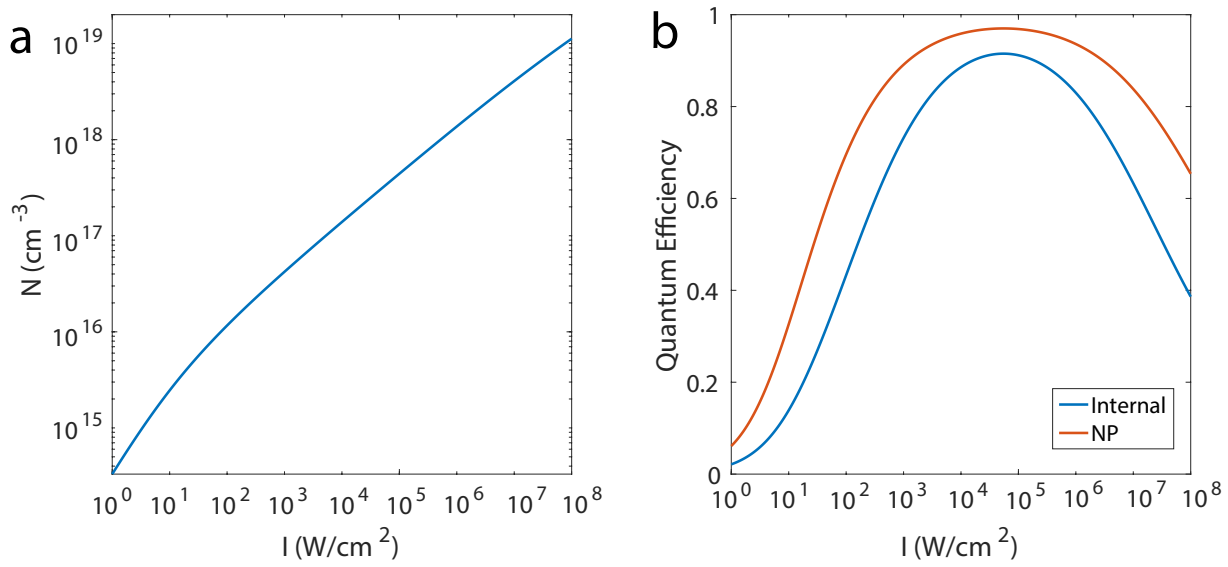

Figure S3: **Carriers generation under illumination.** (a) Light-induced electron-hole pairs density dependence on the illumination laser intensity. (b) Internal quantum efficiency (blue line) and quantum efficiency for resonant nanoparticle (red line)

VII. Surface recombination in perovskite

In addition to bulk monomolecular recombination surface recombination occurs in nanostructures. Value of surface recombination contribution in non-radiative decay A_{surf} equal $1.54 \cdot 10^{-7} s^{-1}$.[S8] Cooling efficiency with taking into account this recombination is as follows:

$$\eta_c = \frac{BF_pN^2}{(A + A_{surf})N + BF_pN^2 + CN^3} \frac{\lambda}{\lambda_{PL}} - 1, \tag{S26}$$

Under resonant conditions (D = 530 nm, λ = 980 nm, I = $7 \cdot 10^6 \frac{W}{cm^2}$) this value will be equal to η_c=7.1%. Without surface recombination ($A_{surf} = 0$) result of cooling efficiency calculation is 7.4%. According Eq.14 from manuscript for particle at the same conditions temperature decrease depends on only cooling efficiency. This means what difference of temperature decrease in this cases is 3%.

VIII. Numerical modelling description

The modeling of the absorption cross-section for $MAPbI_3$ NP on a glass substrate was carried out numerically in a commerical software COMSOL Multiphysics. Light source was taken as plane wave with normal incidence with respect to the glass substrate (n=1.45) with the nanosphere placed on top of it representing the NPs. In our model NP have cut off spherical segment of 50 nm thickness from the bottom. The results in Fig. 4a from the main text were obtained by the integration of the power density in the NP volume.

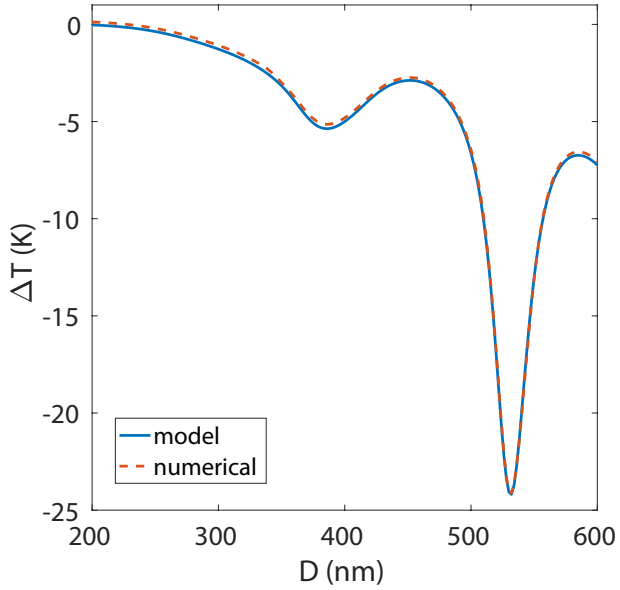

Figure S4: **NPs Temperature.** Temperature change of NP upon laser irradiation of 980 nm wavelength with 10^5 W/cm^2 intensity.

In order to study heat transfer, we use following values: air thermal conductivity κ_{air}=0.022 $\frac{W}{m \cdot K}$, glass thermal conductivity κ_{glass}=1 $\frac{W}{m \cdot K}$ and $MAPbI_3$ thermal conductivity κ_{pero} =0.5 $\frac{W}{m \cdot K}$ [S9]. We define thermal boundary conditions as a heat flux through the computational domain surface $q = h(T_{ext} - T_{surf})$, where h for upper and bottom computational hemispheres are equal to $h_{up} = \kappa_{air}/R_{out}$ and $h_{bottom} = \kappa_{glass}/R_{out}$, respectively, κ is the thermal conductivity, $T_{ext} = 293$ K is the external temperature, T_{surf} is the calculated temperature near boundary of the computational domain, R_{out} - radius of computational domain. Diameter of computational domain is chosen to be 3 μm. Temperature calculations is made without

taking into account thermo-optical nonlinear effects, which might change refractive index and thermal conductivity of heated or cooled materials.

Cooling efficiency from analytical model in air medium was used, in assumption that the effect of the substrate does not significantly vary the emission rate. In order to estimate the performance of the numerical model, calculations of the optical cooling for a spherical NP in homogeneous air media was performed and subsequently compared with the analytical solution (Fig. S4). The calculations are in a complete agreement.

IX. GaAs NP Purcell factor and optical heating calculations

Among others, one of the most popular semiconductor materials in optics and electronics is gallium aresenide (GaAs), owing to high electron mobility and high refractive index in the visible and near-IR which allows it to support optical resonances and strong field localization in nanocavties. However, it's a high-cost and difficult to fabricate material, thus limiting its applicability.

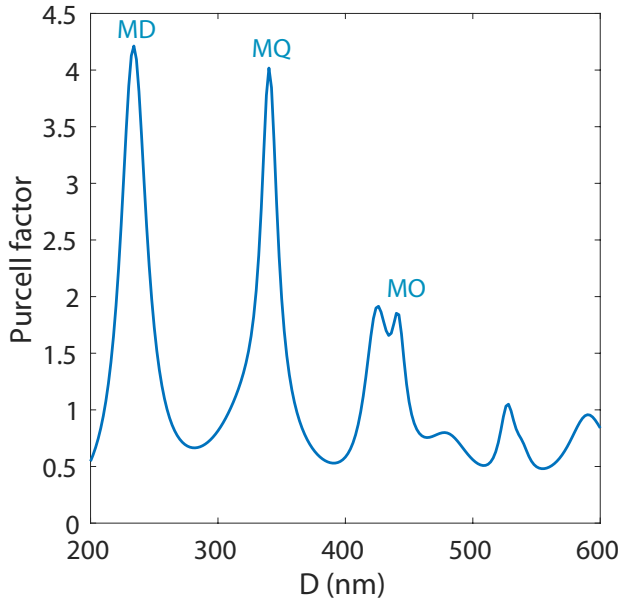

Figure S5: **GaAs Purcell factor.** Calculated Purcell factor for GaAs NP in air for 880 nm wavelength.

Owing to the high refractive index GaAs NPs support high Purcell factor at the photoluminescence wavelength $\lambda_{PL} = 880$ nm in air, as shown in Fig. S5. However, GaAs has a relatively low quantum efficiency and radiative recombination constant[S10,S11]. Therefore, the PL up-conversion cooling approach can not be achieved in such spherical nanocavity. Indeed, Fig. S6a demonstrates calculated temperature dependence of GaAs NP on its diameter and pump wavelength taking into account recombination constants from[S10,S11] (A=$3.8 \cdot 10^7 s^{-1}$, B=$5 \cdot 10^{-11} cm^3 s^{-1}$ and C=$1.5 \cdot 10^{-28} cm^6 s^{-1}$). One can observe no optical cooling for such material and desing, moreover, enhanced heating appears at resonant optical modes excited in the nanocavity. Fig. S6b represents 340 nm diameter NP temperature dependence on

laser intensity with a wavelength of 980 nm. While optical cooling is negligibly low, one can consider temperature increase of the nanoparticle linear with respect to the intensity.

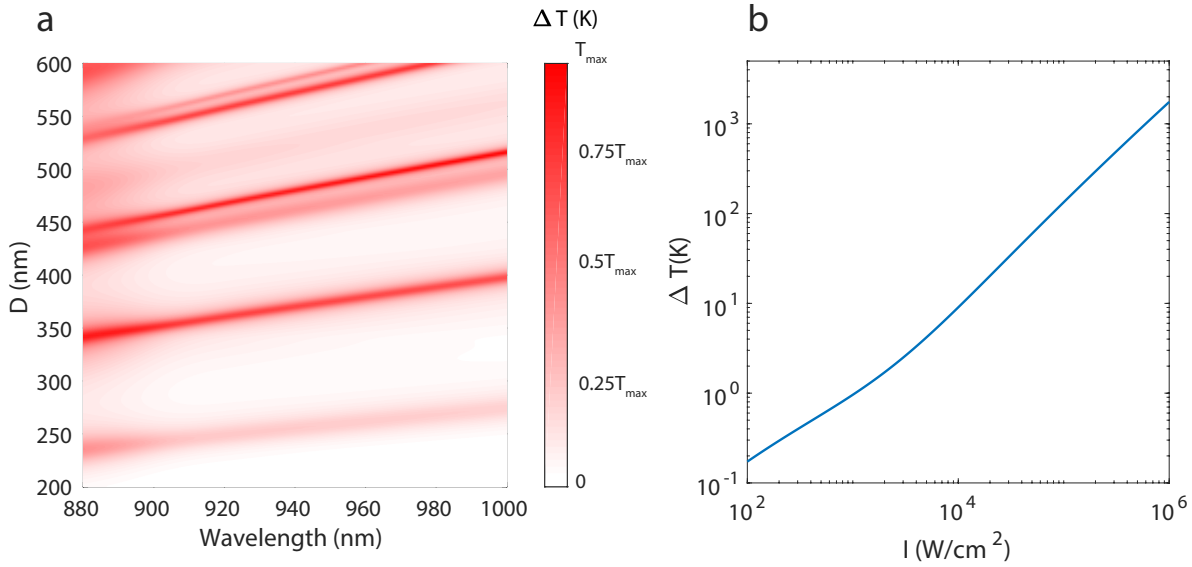

Figure S6: **GaAs NP temperature.** (a) Calculated temperature change of GaAs nanosphere. (b) Calculated temperature change dependence of 340 nm GaAs NP on 980 nm wavelength laser intensity.

X. Numerical modeling for perovskite film

In order to compare optical cooling efficiency of perovskite resonant NP and film on a glass substrate, we carried out numerical calculation in a commercial software COMSOL Multiphysics (2D problem). In the model, we used the same parameters for laser (λ=980 nm, $I = 7 \cdot 10^6 \frac{W}{cm^2}$) as for NP in the main text. The radius of focused beam area is 2 μm. The recombination constants and permittivity for $MAPbI_3$ are the same as for NP calculation. Cooling efficiency was calculated according to the bulk model. The perovskite film thickness is 500 nm. Electric field distribution of normally incident Gaussian beam is demonstrated in Fig. S7a.

For solving heat the transfer problem, we used thermal conductivities and boundary conditions which are described in Part VIII in more details. The size of computational domain was chosen to be 16 μm. The calculated temperature distribution is shown in Fig. S7b exhibiting considerable temperature variation on the scale of a few microns around the focusing spot. Maximal achieved temperature decrease is 16 K. It is worth noting that despite the theoretically obtained value is in a good agreement with previously demonstrated experimental cooling by 23 K for $MAPbI_3$ film[S12], the direct comparison of these result is difficult because work[S12] don't provide all parameters for calculation in our model.

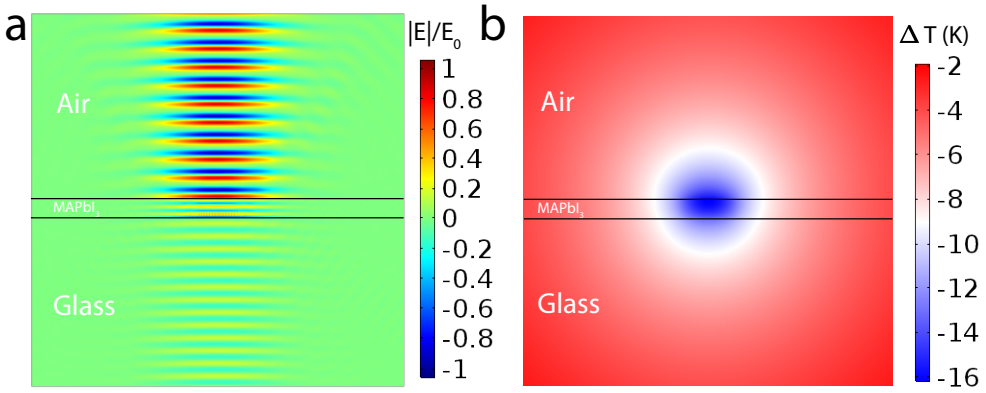

Figure S7: **Optical cooling of perovskite film** (a) Electromagnetic field distribution for Gaussian beam normally fallen on $MAPbI_3$ film. (b) Temperature change distribution under laser irradiation.

References

[S1] Phillips, L. J.; Rashed, A. M.; Treharne, R. E.; Kay, J.; Yates, P.; Mitrovic, I. Z.; Weerakkody, A.; Hall, S.; Durose, K. Dispersion relation data for methylammonium lead triiodide perovskite deposited on a (100) silicon wafer using a two-step vapour-phase reaction process. *Data in brief* **2015**, *5*, 926–928.

[S2] Wang, J.-F.; Zhu, L.; Zhao, B.-G.; Zhao, Y.-L.; Song, J.; Gu, X.-Q.; Qiang, Y.-H. Surface engineering of perovskite films for efficient solar cells. *Scientific reports* **2017**, *7*, 14478.

[S3] Mie, G. Beiträge zur Optik trüber Medien, speziell kolloidaler Metallösungen. *Annalen der physik* **1908**, *330*, 377–445.

[S4] Bohren, C. F.; Huffman, D. R. *Absorption and scattering of light by small particles*; John Wiley & Sons, 2008.

[S5] Chew, H. Radiation and lifetimes of atoms inside dielectric particles. *Physical Review A* **1988**, *38*, 3410.

[S6] Miroshnichenko, A. E.; Evlyukhin, A. B.; Kivshar, Y. S.; Chichkov, B. N. Substrate-induced resonant magnetoelectric effects for dielectric nanoparticles. *Acs Photonics* **2015**, *2*, 1423–1428.

[S7] Permyakov, D.; Sinev, I.; Markovich, D.; Ginzburg, P.; Samusev, A.; Belov, P.; Valuckas, V.; Kuznetsov, A. I.; Luk'yanchuk, B. S.; Miroshnichenko, A. E. *et al.* Probing magnetic and electric optical responses of silicon nanoparticles. *Applied Physics Letters* **2015**, *106*, 171110.

[S8] Yang, M.; Zeng, Y.; Li, Z.; Kim, D. H.; Jiang, C.-S.; van de Lagemaat, J.; Zhu, K. Do grain boundaries dominate non-radiative recombination in CH 3 NH 3 PbI 3 perovskite thin films? *Physical Chemistry Chemical Physics* **2017**, *19*, 5043–5050.

[S9] Heiderhoff, R.; Haeger, T.; Pourdavoud, N.; Hu, T.; Al-Khafaji, M.; Mayer, A.; Chen, Y.; Scheer, H.-C.; Riedl, T. Thermal conductivity of methylammonium lead halide perovskite single crystals and thin films: A comparative study. *The Journal of Physical Chemistry C* **2017**, *121*, 28306–28311.

[S10] t Hooft, G. The radiative recombination coefficient of GaAs from laser delay measurements and effective nonradiative carrier lifetimes. *Applied Physics Letters* **1981**, *39*, 389–390.

[S11] Puhlmann, N.; Oelgart, G.; Gottschalch, V.; Nemitz, R. Minority carrier recombination and internal quantum yield in GaAs: Sn by means of EBIC and CL. *Semiconductor Science and Technology* **1991**, *6*, 181.

[S12] Ha, S.-T.; Shen, C.; Zhang, J.; Xiong, Q. Laser cooling of organic–inorganic lead halide perovskites. *Nature Photonics* **2016**, *10*, 115.